



Publication Year	2015
Acceptance in OA @INAF	2020-04-23T10:52:21Z
Title	The Extreme Ultraviolet Deficit: Jet Connection in the Quasar 1442+101
Authors	Punsly, Brian; MARZIANI, Paola; Kharb, Preeti; O'Dea, Christopher P.; Vestergaard, Marianne
DOI	10.1088/0004-637X/812/1/79
Handle	http://hdl.handle.net/20.500.12386/24198
Journal	THE ASTROPHYSICAL JOURNAL
Number	812

The Extreme Ultraviolet Deficit - Jet Connection in the Quasar 1442+101

Brian Punsly¹, Paola Marziani², Preeti Kharb³, Christopher P. O'Dea^{4,5} and Marianne Vestergaard⁶

ABSTRACT

In previous studies, it has been shown that the long term time average jet power, \overline{Q} , is correlated with the spectral index in the extreme ultraviolet (EUV), α_{EUV} (defined by $F_\nu \sim \nu^{-\alpha_{EUV}}$ computed between 700Å and 1100Å). Larger \overline{Q} tends to decrease the EUV emission. This is a curious relationship because it connects a long term average over $\sim 10^6$ years with an instantaneous measurement of the EUV. The EUV appears to be emitted adjacent to the central supermassive black hole and the most straightforward explanation of the correlation is that the EUV emitting region interacts in real time with the jet launching mechanism. Alternatively stated, the \overline{Q} - α_{EUV} correlation is a manifestation of a contemporaneous (real time) jet power, $Q(t)$, correlation with α_{EUV} . In order to explore this possibility, this paper considers the time variability of the strong radio jet of the quasar 1442+101 that is not aberrated by strong Doppler enhancement. This high redshift ($z = 3.55$) quasar is uniquely suited for this endeavor as the EUV is redshifted into the optical observing window allowing for convenient monitoring. More importantly, it is bright enough to be seen through the Lyman forest and its radio flux is strong enough that it has been monitored frequently. Quasi-simultaneous monitoring (five epochs spanning ~ 40 years) show that increases in $Q(t)$ correspond to decreases in the EUV as expected.

Subject headings: Black hole physics — magnetohydrodynamics (MHD) — galaxies: jets—galaxies: active — accretion, accretion disks

¹1415 Granvia Altamira, Palos Verdes Estates CA, USA 90274 and ICRANet, Piazza della Repubblica 10 Pescara 65100, Italy, brian.punsly1@verizon.net

²INAF, Osservatorio Astronomico di Padova, Italia

³Indian Institute of Astrophysics, II Block, Koramangala, Bangalore 560034, India

⁴Department of Physics and Astronomy, University of Manitoba, Winnipeg, MB R3T 2N2 Canada

⁵School of Physics & Astronomy, Rochester Institute of Technology, Rochester, NY 14623, USA

⁷Dark Cosmology Centre, Niels Bohr Institute, University of Copenhagen, Juliane Maries Vej 30, DK-2100 Copenhagen ϕ , Denmark

1. Introduction

Powerful relativistic radio jets have been associated with the most intrinsically luminous ultraviolet emitters in the Universe, namely quasars, since their discovery over 50 years ago. Only a small fraction of all quasars ($\sim 10\%$) have strong jets (radio loud quasars RLQs), and even fewer have radio lobes on super-galactic scales, $\sim 1.7\%$ of all quasars have such extended structure (deVries et al. 2006). However, until recently there has been no observations of the jet launching region, so there has been much speculation as to the mechanism that creates these jets. The literature is filled with numerical models and theories (Lovelace 1976; Blandford and Znajek 1977; Blandford and Payne 1982; Punsly 2008). There is no discriminant for authenticity due to a lack of direct measurement of the jet launching region. However, this has changed recently with the examination of extreme ultraviolet (EUV) spectra shortward of the peak of the spectral energy distribution (SED) at 1100\AA . The quasar luminosity is widely believed to arise from the viscous dissipation of turbulence driven by the differential rotational shearing of accreting gas (Lynden-Bell and Rees 1971; Shakura and Sunyaev 1973). In numerical and theoretical models, the highest frequency optically thick thermal emission arises from the innermost region of the accretion flow and its frequency is shortward of the peak of the SED (Zhu et al. 2012). The EUV spectrum beyond the peak of the SED of quasars is the putative Wien tail of the emission of the innermost thermal component of the accretion flow that is adjacent to the central black hole (Marshall et al. 1997; Punsly 2014). If \overline{Q} is the long term ($\sim 10^6$ years) time averaged jet power (as determined from radio lobe emission and morphology), and L_{bol} is the bolometric thermal emission associated with the accretion flow, it was shown in Punsly (2014, 2015b) that jet efficiency, \overline{Q}/L_{bol} , (which depends on a long term average) was correlated with the deficit of EUV emission in RLQs relative to radio quiet quasars quantified by α_{EUV} (the flux density scales as $F_\nu \propto \nu^{-\alpha_{EUV}}$ and is computed between 1100\AA and 700\AA). This is the fundamental correlation and a partial correlation analysis shows that the correlation that exists between \overline{Q} and α_{EUV} is spurious (Punsly 2015b). This provides the first connection between jet power and an observable from a region that is likely contiguous or coincident with the jet launching region in quasars.

This is a curious circumstance since the plasma in the radio lobes that is used to determine \overline{Q} was ejected from the central engine $\sim 10^6$ years before the EUV emitting gas reached the environs of the central black hole. Two parameters, L_{bol} and α_{EUV} are “real time” diagnostics of the quasar at the time of observation and \overline{Q} is a long term time average. Why should these parameters be connected in what is likely a time variable system? It was concluded based on a statistical argument that the most logical explanation is that there is an underlying real time connection between the instantaneous jet power, $Q(t)$, and α_{EUV} (Punsly and Marziani 2015). It is too much of a coincidence that two highly dynamic

elements emanating from a common region are strongly correlated if there is no real time connection. The scatter seen in the correlation (see Figure 1) includes the variation of L_{bol} and α_{EUV} from their long term time average value and the degree of scatter indicates that in general these variations are modest.

In this paper, a search is initiated for the real time connection between $Q(t)/L_{bol}$ and α_{EUV} . This is a daunting task since it is not trivial to find an estimator that scales with $Q(t)$ that is reliable and there is simply not enough observing time on the *Hubble Space Telescope* (HST) to monitor quasar continua (spectra are needed to excise the emission lines) in the EUV. Sufficient monitoring requires observing a source with earth-based telescopes which requires $z > 3$ in order to get the EUV redshifted into the U or B bands. This is not ideal due to the large flux attenuation by the intervening Ly α forest. Firstly, the quasar must have an incredibly large intrinsic EUV luminosity in order to shine bright enough to be seen easily through the absorbing screen. The second requirement is that the radio luminosity should be high enough so that the object appears frequently in survey work so that there is an ample database to cull through for quasi-simultaneous observations. The third requirement is almost mutually exclusive from the first two. In order to monitor $Q(t)$ by radio flux, the source cannot suffer from Doppler aberration. This is necessary since small variations in geometry would appear as significant changes in the observed flux and this would provide a false indicator of changes in the intrinsic jet luminosity (Lind and Blandford 1985). Most of the radio sources at $z > 3$ in the older radio catalogs have sufficient flux density because they are Doppler enhanced. Thus, we have a very strong set of restrictions due to the high redshift, luminosity and lack of Doppler beaming: the source needs an enormous intrinsic radio luminosity with no significant Doppler beaming (i.e. $\sim 1\text{Jy}$ at $z > 3$ with no Doppler beaming). Do such sources exist? They seem to in the form of gigahertz peak radio sources (GPS). Some of these at high redshift are incredibly luminous (O’Dea 1998). We argue below that the quasar 1442+101 at $z = 3.55$ is a suitable candidate.

2. Source Selection

The high redshift quasar, 1442+101, is a powerful radio source that appeared in many of the early radio surveys. The spectrum peaks at $\approx 1\text{ GHz}$ at 2.5 Jy . Therefore, it was very surprising that the source was at extremely high redshift. It was also surprising that unlike other high redshift sources that appear in radio surveys, it is not blazar-like in that it is not highly variable at radio frequencies.

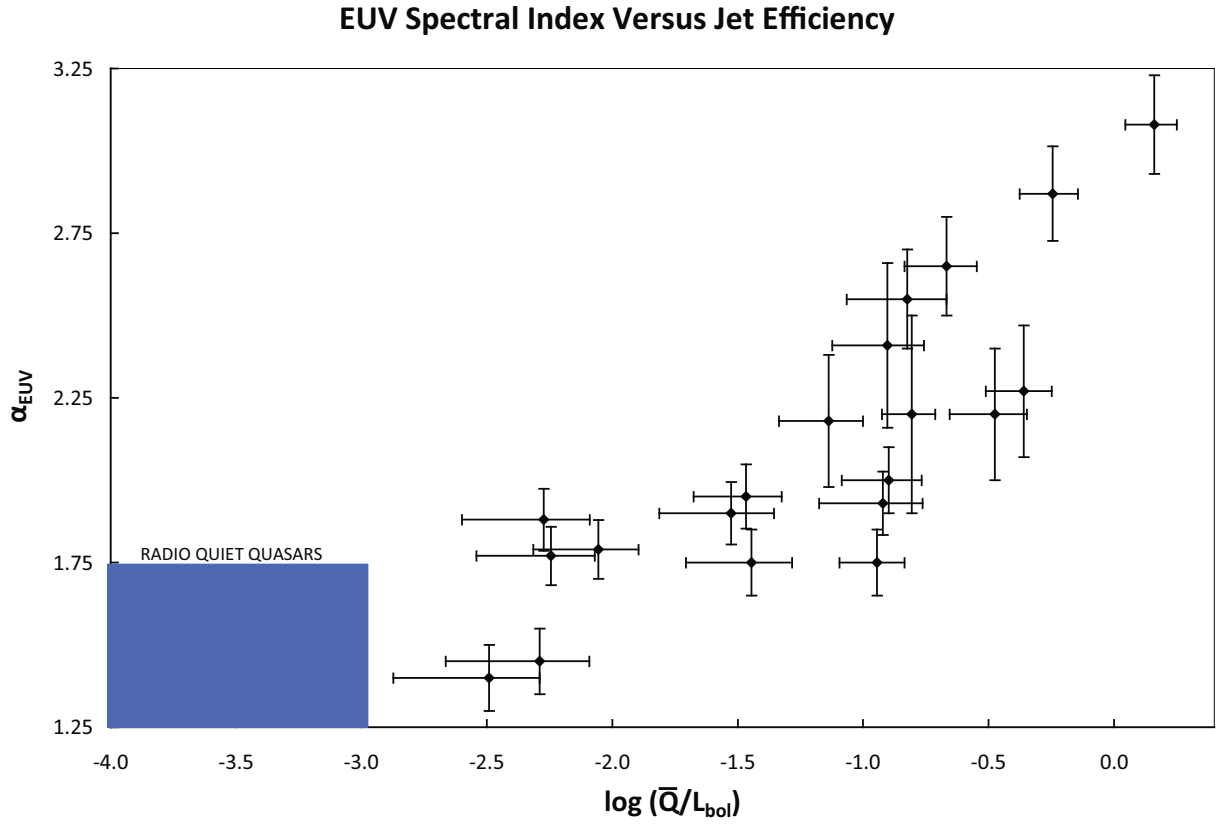


Fig. 1.— The correlation of α_{EUV} versus the jet efficiency, \bar{Q}/L_{bol} (Punsly 2015b; Punsly and Marziani 2015). More powerful jets have depressed EUV emission.

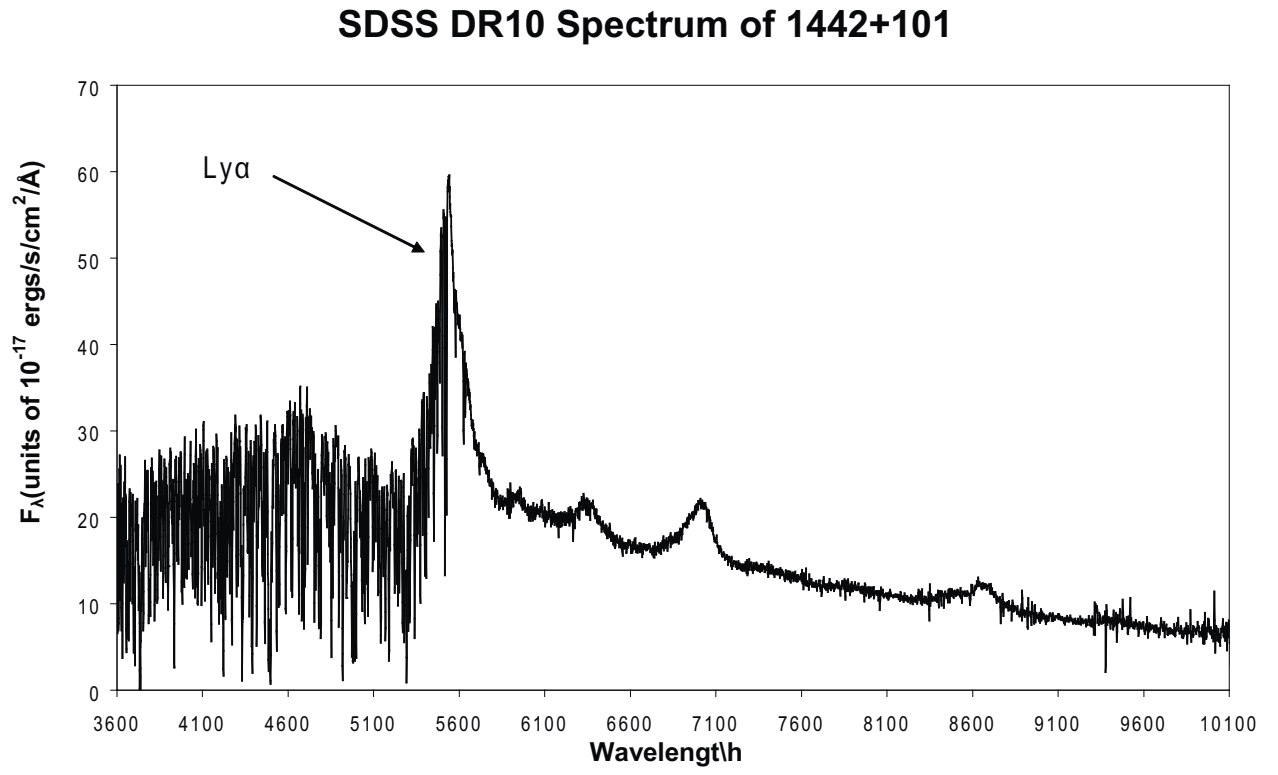


Fig. 2.— Note the ample flux shortward of Ly α in the SDSS DR 10 spectrum of 1442+101.

2.1. Doppler Beaming

It is argued here that the radio emission at frequencies below 10 GHz is not Doppler beamed in 1442+101. A list of evidence of Doppler beaming occurs below. For each item in the list, the actual circumstance observed in 1442+101 is listed after the colon.

1. Extreme radio variability: Not evident in the large dataset compiled in the NASA Extragalactic Database or the monitoring in Tingay et al (2003); Mingaliev et al. (2012). This is indicative of non-blazar radio emission.
2. Superluminal motion on 30 pc - 100 pc scales: There is no measurable change in position of the three components seen at 1.6 GHz VLBI images in 1989 and in the 2.3 GHz VLBI images from 1999 on scales of 10 pc - 100 pc (Dallacasa et al. 1995; Pushkarev and Kovalev 2012). No blazar-like pc scale evolution has been observed.
3. Flat spectrum radio core to > 30 GHz in the quasar rest frame: The spectrum is very steep with a spectral index $\alpha > 1$ above 30 GHz in the quasar rest frame (Kovalev et al. 1999; Mantovani et al. 2009). The spectrum continues to steepen towards 1000 GHz in the quasar rest frame (Steppe et al 1995). Thus, there is no “buried” flat spectrum core embedded within the source of the gigahertz peaked emission. There is insignificant blazar-like synchrotron self-absorption at high frequency.
4. Large optical variability: Low optical variability is reported (Pica et al. 1988; Smith et al. 1993). The optical variability is similar to radio quiet quasars and thus not typical of blazars.
5. Large optical polarization: No measurements exist. Inconclusive evidence of blazar activity.

The preponderance of evidence indicates that Doppler beaming does not affect the emission from 1442+101 significantly.

2.2. Estimator for $Q(t)$

If a source is not Doppler beamed then it seems reasonable to choose the optically thin radio luminosity created in the most compact regions of the source as a quantity that scales with jet power. This emanates inside of any working surface (a region of intense jet dissipation such as an interaction with a dense cloud) and without synchrotron - self absorption, we are looking directly at the synchrotron emission that directly reflects dynamical elements,

the energy of electrons and the energy of the magnetic field in the jet. It might not be a linear relationship, but increases in the optically thin radio emission from the innermost jet should be positively correlated with the jet power. The quasar 1442+101 is one of the most compact radio sources known (van Breugel et al. 1984). There is no emission, even in deep observations, on kpc scales (Murphy et al. 1993). Based on VLBI (very long baseline interferometry) images of GPS quasars at lower redshift (higher spatial resolution than is possible with 1442+101 observations), the radio emission is highly resolved with a small fraction in the core unlike blazars (Stanghellini et al. 1997, 2001). Most of the emission especially at lower frequencies comes from knots in the jet > 10 pc from the core, the putative working surface. This is the primary source of the optically thick low frequency emission in most GPS quasars and likely 1442+101 as well. To estimate $Q(t)$, it is not appropriate to sample the optically thick radio emission from the “working surface” that depends on dissipation that is determined by dynamics and physical conditions external to the jet. Above 8.4 GHz (observer frame) the spectral index is $\alpha > 1$ (optically thin) and this frequency is sampled frequently (Kovalev et al. 1999; Mantovani et al. 2009; Mingaliev et al. 2012). Thus, the 8.4 GHz flux density should be an indicator of jet strength well inside the working surface. VLBI imaging at 8.6 GHz indicates that the majority of the 8.4 GHz flux is unresolved inside of 50 light years from the source (Pushkarev and Kovalev 2012). This is the surrogate to monitor jet power given the insufficient monitoring at higher frequencies.

2.3. EUV Penetration of the Lyman Forest

The most startling aspect of 1442+101 is that the EUV emission is so bright that it shines through a dense forest of $\text{Ly}\alpha$ absorbing clouds. The spectrum in Figure 2 indicates that there is more than adequate luminosity to sample the spectrum at $\lambda_o = 4000 \text{ \AA}$ (observer frame) corresponding to $\lambda_e = 880 \text{ \AA}$ in the quasar rest frame. The flux measured is not the intrinsically emitted flux, but that attenuated by the Lyman forest. About five or six absorbers have been resolved spectroscopically in a $\delta\lambda_o = 100 \text{ \AA}$ window centered at $\lambda_o = 4000 \text{ \AA}$ (Baldwin et al. 1974; Barthel et al. 1990). The intervening gas is comprised of many small absorbing clouds, so one does not expect significant time variation in the total flux integrated over a 100 \AA window due to changes in the total absorbing column. By measuring the EUV continuum at $\lambda_e = 880 \pm 11 \text{ \AA}$ we avoid contamination by emission lines (Telfer et al. 2002). The 100 \AA “smoothing” window minimizes any affects caused by spectral resolution differences between observations and the narrow absorption lines, allowing for a consistent method of determining the observed flux density at $\lambda_o = 4000 \text{ \AA}$.

3. Results

There are far more radio observations than calibrated optical spectra down to $\lambda_o = 4000\text{\AA}$. The optical and radio variability is small (Pica et al. 1988; Tingay et al 2003). Due to the paucity of optical data sampling it thus seems reasonable (but not ideal) to consider observations within 300 days as quasi-simultaneous. Due to cosmological redshifting, this corresponds to about 66 days in the quasar rest frame. To put this in perspective, we estimate the size of the putative active EUV/radio emitting region in 1442+101 as follows. Based on standard bolometric corrections, Figure 2 and archival IR (rest frame optical) data from the NASA Extragalactic Database, we estimate $L_{bol} \approx 4 - 5 \times 10^{47}$ ergs/sec, ignoring the contribution from reprocessed emission (avoiding double counting) in the molecular clouds (Punsly 2015b; Davis and Laor 2011). If the accretion flow is radiating at $< 50\%$ of the Eddington rate, the black hole mass would be $M_{bh} > 8 \times 10^9 M_\odot$. For a rapidly spinning black hole, 66 days corresponds to < 2 Keplerian orbital periods at a distance of $5R_g$ ($R_g > 1.1 \times 10^{15}$ cm is the black hole radius for a rapidly rotating black hole) from the central black hole in the equatorial plane. This also corresponds to < 4 Keplerian orbital periods at a distance of $3R_g$ from the central black hole in the equatorial plane. These are reasonable estimates for the location of the EUV emitting region from the variability of the EUV and numerical models of accretion flows (Marshall et al. 1997; Haba et al 2003; Zhu et al. 2012; Punsly 2014, 2015b). Thus, 300 days is not that unreasonable of a condition for quasi-simultaneity in the context of jet production and EUV emission.

Table 1 shows the data for the 5 quasi-simultaneous epochs that are spread out over ~ 40 years (1973 - 2012). Table 1 lists the date of observations (column 1), the 8.46 GHz flux density (column 2), the flux density at $\lambda_o = 4000\text{\AA}$ (column 3), the telescopes (column 4), the difference in the observation date from the optical and radio in days (column 5) and the references (columns 6 and 7). For observations that are at a slightly different frequency than 8.46 GHz ($\sim 100 - 400$ MHz), a spectral index of 1 is assumed based on the MJD 47266 VLA observations at 8.21 GHz and 8.66 GHz and archival data (Kovalev et al. 1999; Mingaliev et al. 2012; Mantovani et al. 2009). We note that the observation in Barthel et al. (1990) on MJD 47320 in Table 1 is chosen to have the largest fractional uncertainty, 15%, of all the epochs. Issues with the flux calibration have been noted based on the atmospheric dispersion correction for the Barthel et al. (1990) sample (Corbin 1991). For SDSS DR10 quasar data, such as the MJD 55976 observation in Table 1, there is a calibration issue in the blue part of the spectrum. Specifically, in order to increase spectral sensitivity for quasars, the hole drilled over the aperture is centered on the displacement associated with 4000\AA . However, the calibration of the star has a hole centered about the displacement associated with 5400\AA . This inconsistency artificially raises the flux level in the blue that we estimate as a 7.2% excess for quasar light at 4000\AA (from the airmass of 1.1 and seeing of 1.4 arcsec).

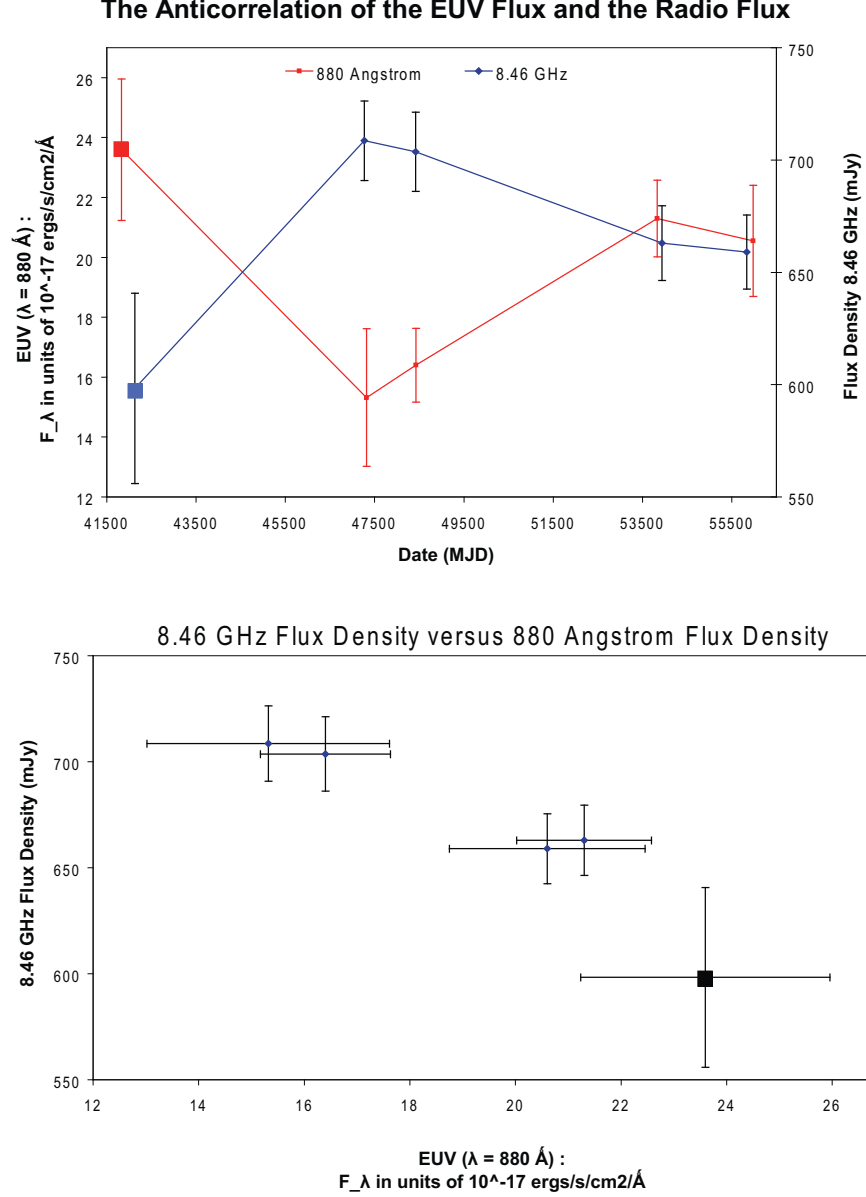


Fig. 3.— The top frame shows the light curves for EUV flux density and 8.46 GHz flux density sampled at quasi-simultaneous observation epochs. The bottom frame shows the anti-correlation of the EUV flux density and the 8.46 GHz flux density. The squares indicate the observational epoch that is not in the “gold sample” (not a VLA radio observation) described in the text.

Table 1: Quasi-simultaneous EUV and Radio Variability of 1442+101

Observation Date (MJD) Radio/ Optical	Flux Density 8.46 GHz (mJy)	Flux Density $\lambda_o = 4000 \text{ \AA} (\lambda_e = 880 \text{ \AA})$ (10^{-17} ergs/sec/cm ² /Å)	Telescope Radio/ Optical	Delta ^a (Days)
42126/ 42189	598 ± 42 ^b	23.4 ± 2.4 ^c	Parkes 64m/ Lick 3m	297
47266/ 47320	709 ± 18 ^d	15.3 ± 2.3 ^e	VLA/ Hale 5m	54
48415/ 48427	704 ± 18 ^d	16.4 ± 1.2 ^f	VLA/ Lick 3m	12
53940/ 53827	663 ± 16 ^d	21.3 ± 1.3 ^d	VLA/ SDSS DR7	113
55834/ 55976	659 ± 16 ^d	20.5 ± 1.4 ^d	VLA/ SDSS DR10	142

^aNumber of days between radio and optical observations

^bShimmins and Bolton (1981)

^cBaldwin et al. (1974)

^dThis paper

^eBarthel et al. (1990)

^fLyons et al. (1995)

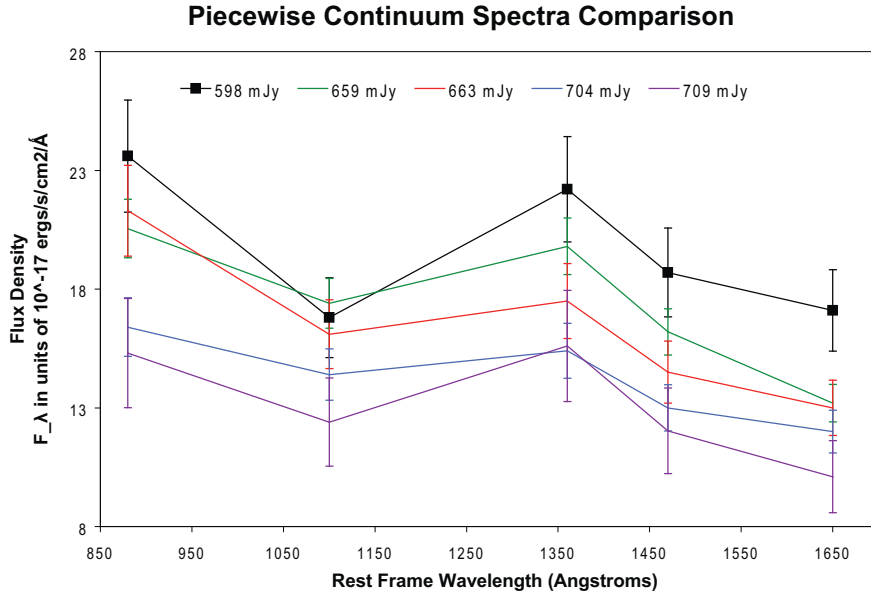


Fig. 4.— The piecewise continuum estimates in the far UV and EUV of the different epochs labeled by their 8.46 GHz flux density. The squares indicate the observational epoch that is not in the “gold sample” (not a VLA radio observation) described in the text. The continuum excess of weak jet states relative to strong jet states is largest in the EUV.

If there is a similar underestimate of the standard star flux at 4000\AA , the total estimated increase in the DR10 quasar spectral flux is 14.4% at 4000\AA . As a check of this calculation, we note that this agrees with the offset seen between the photometric g magnitude and the synthetic magnitude computed from the spectrum (18.61 and 18.39, respectively). The corrected spectrum is plotted in Figure 2.

Table 1 can be used to assess the real time connection between $Q(t)/L_{bol}$ and α_{EUV} . Notice that, per the discussions by Punsly (2015b), $L_{bol} \approx 3.8F_{\lambda_e}(\lambda_e = 1100\text{\AA})$ in the quasar rest frame and $\alpha_{EUV} = \log \frac{F_{\lambda_e}(\lambda_e=880\text{\AA})}{F_{\lambda_e}(\lambda_e=1100\text{\AA})} / \log \frac{1100\text{\AA}}{880\text{\AA}}$.¹ Thus, α_{EUV} varies monotonically with $F_{\lambda_e}(\lambda_e = 880\text{\AA})/F_{\lambda_e}(\lambda_e = 1100\text{\AA})$. If there is a relationship between $Q(t)/L_{bol}$ and α_{EUV} then there is a relationship between $Q(t)/L_{bol}$ and $F_{\lambda_e}(\lambda_e = 880\text{\AA})/F_{\lambda_e}(\lambda_e = 1100\text{\AA})$. The advantage of the latter relationship is that both quantities have $F_{\lambda_e}(\lambda_e = 1100\text{\AA})$ in the denominator. Thus if one multiplies both quantities by $F_{\lambda_e}(\lambda_e = 1100\text{\AA})$, one only needs to look at the light curves of $Q(t)$ (as traced by the 8.46 GHz flux density) and $F_{\lambda_o}(\lambda_o = 4000\text{\AA})$ (equivalently $F_{\lambda_e}(\lambda_e = 880\text{\AA})$) in order to detect a correlation between $Q(t)/L_{bol}$ and α_{EUV} . The motivation for this re-normalization is to remove the undesirable statistical scatter caused by dividing both the quantities by $F_{\lambda_o}(\lambda_o = 5000\text{\AA})$ (corresponding to $\lambda_e = 1100\text{\AA}$) that adds to each measured quantity considerable uncertainty, but does not add physical content. Such an expedience would not be justified in an analysis that comprised multiple objects since each object is normalized differently and the normalization is time variable.

The top frame of Figure 3 is a plot of both 8.46 GHz flux density and $F_{\lambda_o}(\lambda_o = 4000\text{\AA})$ as a function of time. The bottom frame of Figure 3 shows that $Q(t)$ decreases as $F_{\lambda_o}(\lambda_o = 4000\text{\AA})$ increases as expected. Even though the number of observations is too small for rigorous statistical analysis, we note that Pearson correlation coefficient is -0.949 corresponding to a one-sided 99.3% statistical significance. If one restricts the analysis to a “gold sample” of epochs all observed with the same telescope (the VLA) and within 150 days of the optical observation (< 2 Keplerian orbits $3R_g$ from the black hole), one still sees a correlation. The two stronger radio states have the weakest $F_{\lambda_o}(\lambda_o = 4000\text{\AA})$ and vice versa for the two weaker radio states.

In the analysis of HST composite spectra in Punsly (2014); Telfer et al. (2002), a deficit of EUV continuum emission was associated with the radio loudness in quasars. There was no deficit of emission seen in the far UV continuum for RLQs. However, the continua plotted in Figure 4 indicate a far UV continuum suppression as the jet gets stronger. The plot

¹Our spectra do not extend all the way to $\lambda_e = 700\text{\AA}$. A power law fits the continuum well in this range for other quasars (Punsly 2015b). Using $\lambda_e = 880\text{\AA}$ to compute the power law should be an adequate expedience to see changes in spectral slope.

shows piecewise continuum spectra estimates in the far UV and EUV at the different epochs labeled by their 8.46 GHz flux density. The rest frame points were sampled at wavelengths in which line emission seemed minimal in all the spectra. Rest frame wavelengths were indicated for ease of comparison to well known emission lines. The observed wavelengths are 4000 Å, 5000 Å, 6200 Å, 6700 Å, and 7500 Å. There are three radio “weaker” jet states at 598 mJy, 659 mJy, 663 mJy and two “stronger” jet states at 704 mJy and 709 mJy. The UV fluxes are highly clustered at $\lambda_e = 1650\text{\AA}$, four of the flux density measurements are not statistically significantly different. The flux density of the continua associated with the weak jet states exceeds that of the continua associated with the strong jet states by an ever increasing differential as the wavelength decreases. Furthermore, the EUV spectra from 1100Å to 880Å are softer (larger α_{EUV}) for the stronger jet states than for the weaker jet states as expected from a $Q(t)/L_{bol}$ and α_{EUV} correlation. The continuum suppression associated with jet power might taper off in the far UV as opposed to an abrupt turn off at $\lambda_e = 1100\text{\AA}$.

4. Discussion

The physical interpretation of the correlation between jet power and the decrement in EUV luminosity that is illustrated in Figure 1, 3 and 4 was elucidated in two previous studies (Punsly 2014, 2015b). In this section, we review this analysis and discussion in order to put the results into perspective. The most straightforward explanation of the correlation involves jets from magnetic flux in the inner accretion disk where the EUV emission also originates. As more poloidal vertical magnetic flux is stored in the innermost accretion disk, the volume available for the thermal emitting gas is displaced. More poloidal magnetic flux equates to a stronger jet and less optically thick thermal gas equates to a weaker EUV luminosity. This dynamical configuration is known as magnetically arrested accretion (Igumenshchev 2008).

Many different dynamical systems have been classified as magnetically arrested in the numerical simulation literature. The relevant numerical simulations for RLQs are the ones in which the vertical magnetic flux is distributed in magnetic islands of low plasma density that are concentrated in the inner accretion flow. The configuration is far from time stationary. The islands are dynamic and buoyantly move through the ram pressure imposed by the dense thermal EUV emitting plasma by means of a series of Kruskal-Schwarzschild instabilities (Igumenshchev 2008). The ram pressure of the accretion flow concentrates magnetic flux near the black hole.

4.1. A Review of Evidence for Magnetically Arrested Accretion in RLQs

Evidence of the detailed predictions of magnetically arrested accretion was found in Punsly (2015b) by exploring a basic model. The first prediction is that due to the ram pressure interaction of the accreting gas with the magnetic islands, the correlation of \overline{Q}/L_{bol} and α_{EUV} should be stronger than the correlation between \overline{Q} and α_{EUV} . This was verified by a partial correlation analysis that indicated that the correlation of \overline{Q}/L_{bol} with α_{EUV} is statistically significant and the correlation of \overline{Q} with α_{EUV} is spurious.

The second piece of evidence supporting magnetically arrested accretion that was found in Punsly (2015b) is a verification of the specific relationship between the jet power and the EUV suppression that arises from the basic model of magnetically arrested accretion. The derivation will not be repeated here, but the introduction of some notation is required to explain the exact result that was demonstrated. If the model is representative of the physical circumstance depicted in Figure 1 then the filling fraction of the inner accretion disk with magnetic islands, f , is related to the deficit of EUV luminosity, where the EUV luminosity deficit is evaluated relative to luminosity of the EUV continuum of radio quiet quasars (RQQs). In order to compare the EUV deficit from object to object, the EUV spectral luminosity was normalized in Punsly (2015b) to the spectral luminosity at the approximate peak of the spectral energy distribution (SED),

$$\text{Normalized EUV Spectral Luminosity} \equiv \frac{L_\nu(\lambda = 700\text{\AA})}{L_\nu(\lambda = 1100\text{\AA})}, \quad (1)$$

where $L_\nu(\lambda = 700\text{\AA})$ is the EUV continuum spectral luminosity and $L_\nu(\lambda = 1100\text{\AA})$ is the spectral luminosity at the approximate peak of the SED. Defining the EUV deficit of a RLQ relative to RQQs requires defining a fiducial normalized EUV spectral luminosity for RQQs from composite spectra (Punsly 2015b)

$$\text{Fiducial Normalized EUV Spectral Luminosity} \equiv \left. \frac{L_\nu(\lambda = 700\text{\AA})}{L_\nu(\lambda = 1100\text{\AA})} \right|_{\text{RQQ}}, \quad (2)$$

where $L_\nu(\lambda = 700\text{\AA})$ is the EUV continuum spectral luminosity of the RQQ composite spectrum and $L_\nu(\lambda = 1100\text{\AA})$ is the spectral luminosity at the approximate peak of the SED in the RQQ composite spectrum. The normalized EUV deficit is approximately equal to the magnetic flux fill fraction, f , of the inner disk (equivalently the fractional volume of EUV emitting gas that is displaced by magnetic flux tubes) in each individual RLQ

$$\text{EUV Deficit} \equiv \left[1 - \left[\frac{L_\nu(\lambda = 700\text{\AA})}{L_\nu(\lambda = 1100\text{\AA})} \right] \left[\frac{L_\nu(\lambda = 1100\text{\AA})}{L_\nu(\lambda = 700\text{\AA})} \right] \right|_{\text{RQQ}} \right] \approx f. \quad (3)$$

Since the jet power scales with the square of the poloidal magnetic flux contained within the jet base, the scaling that is predicted by the basic model of magnetically arrested accretion was shown by Punsly (2015b) to be of the form

$$\overline{Q}/L_{\text{bol}} \approx Af^2 \approx A \left[1 - \left[\frac{L_\nu(\lambda = 700\text{\AA})}{L_\nu(\lambda = 1100\text{\AA})} \right] \left[\frac{L_\nu(\lambda = 1100\text{\AA})}{L_\nu(\lambda = 700\text{\AA})} \right] \Big|_{\text{RQQ}} \right]^2, \quad (4)$$

where A is a constant. The best fit to the RLQ data was found to be

$$\overline{Q}/L_{\text{bol}} = A \left[1 - \left[\frac{L_\nu(\lambda = 700\text{\AA})}{L_\nu(\lambda = 1100\text{\AA})} \right] \left[\frac{L_\nu(\lambda = 1100\text{\AA})}{L_\nu(\lambda = 700\text{\AA})} \right] \Big|_{\text{RQQ}} \right]^{2.05 \pm 0.17}. \quad (5)$$

The uncertainty in the exponent includes uncertainty in the fiducial RQQ normalized EUV spectral luminosity in Equation (2) as well as the statistical scatter in the data. The agreement of the exponent in equations (4) and (5) within these uncertainties provides strong evidence that the mechanism that is creating the jet and suppressing the EUV emission is in fact similar to magnetically arrested accretion in the innermost accretion disk. It is further estimated from the same analysis that f is a few percent for the RLQs with weaker jets and $\sim 50\%$ for the RLQs with the most powerful jets (Punsly 2015b; Punsly and Marziani 2015).

4.2. Review of the EUV Deficit in the Context of Numerical Simulations

A major shortcoming of 3-D numerical models of accretion onto black holes is that the magnetic field topology and poloidal flux distribution is determined by physics beyond the assumed single fluid ideal magnetohydrodynamic (MHD) approximation. This is critical because it has been shown that even small changes in the numerics near the black hole will drastically alter the poloidal magnetic flux topology and the entire dynamical scheme (Punsly 2015a). Most prominent amongst these missing features is the microphysics that determines the diffusion rate of plasma onto and off of magnetic field lines and the magnetic field reconnection rate. Neither of these are well known in the exotic environment near black holes. These physical processes are critical not only for the formation of the magnetic islands, but the time evolution of the magnetic islands is determined primarily by diffusion (Igumenshchev 2008; Punsly 2015a). Even worse, these dynamical elements occur only as a consequence of numerical diffusion in modern simulations in over simplified ideal MHD single fluid models of the physics (Punsly 2015a). Future development is difficult since it is not even clear theoretically what the basic principles required for an accurate physical depiction would be. Many issues that are related to these topics are active areas of investigation in solar and fusion physics (Bauman et al 2013; Malakit 2009; Threlfall et al. 2012; Yamada

2007). As such it is imperative that observational results such as those presented here are needed to guide the course of numerical and theoretical work.

The observational evidence provided by this study can be used to cull through possible numerical and physical scenarios in order to see which ones are viable candidates to represent the physical system in a RLQ. The following restrictions for numerical work are model independent and derive directly from the observations (Punsly 2015b). These can be used to guide us toward numerical models that replicate the physics of jet launching in RLQs. Empirically, it is determined that both the large scale poloidal magnetic flux at the base of the jet and a mechanism that suppresses (but does not eliminate) the EUV emission from the innermost accretion flow coexist at the heart of the central engine of RLQs. This is too large of a coincidence, some of this magnetic flux must be the same element that disrupts, but does not eliminate the innermost accretion flow. This implies that there is significant vertical poloidal magnetic flux in the inner accretion flow of RLQs. If a numerical effort cannot reproduce this circumstance then perhaps the numerical approximation to the relevant physical processes requires further development. Observations are now mature enough to lead the numerical work.

Summarizing the status of the numerical work, it is noted that the magnetically arrested accretion discussed above in the introduction to this section is qualitatively similar to the 3-D numerical simulations explored in Igumenshchev (2008) and Punsly et al. (2009). They produce a fill fraction, f , in the innermost accretion flow that is consistent with the range described below Equation (5). They also provide most of the gross features of time evolution required to support the jets and suppress the EUV emission in the innermost accretion flow (Punsly 2015b). By contrast, the simulations in McKinney et al. (2012); Tchekhovskoy et al. (2011, 2012) that are heavily seeded with large scale magnetic flux are devoid of magnetic islands close to the event horizon. This is evidenced by the claim in McKinney et al. (2012) that no significant Poynting flux emerges from this region as well as the linked online videos of the simulations. The videos show the innermost significant, modest, magnetic island concentrations are located at $r > 10R_g$ and they are extremely transient. In McKinney et al. (2012); Tchekhovskoy et al. (2011, 2012) the fill fraction, $f \approx 0$ in the innermost accretion flow. This is basically a zone of avoidance for vertical poloidal magnetic flux in these simulations. Instead of penetrating the thickness of the equatorial accretion flow, vertically, the poloidal field spreads out above and below the accretion disk in radial fans. Thus, these simulations are not consistent with the observations of RLQs. These radial fans compress or “choke” the flow. The “magnetically choked accretion flows” of McKinney et al. (2012) heat the innermost accretion flow compressively as part of the magnetic choking process and likely increase radiation from this region. This is verified by the recent results from this family of simulations (Avara et al. 2015). The inner accretion flow luminosity is claimed to

increase significantly over a standard optically thick, geometrically thin accretion disk, the opposite of what is observed in RLQs.

4.3. The EUV Deficit and Jet Formation Across all Scales

It is tempting to put these results into a broader context. It is possible that all black hole related jet phenomena are a consequence of vertical magnetic flux impeding the inner accretion flow. In particular, for Galactic black hole binaries (GBH) jet type emission occurs only when the soft X-ray emission (the putative thermal emission from the accretion disk) is suppressed (Russell et al 2011; Fender et al 2004; Klein-Wolt et al 2002). However, the “coronal” X-ray power law emission is not suppressed and can be very strong (Punsly and Rodriguez 2013; Fuchs et al 2003).

There have also been claims that dips in the coronal X-ray flux (the X-ray power law) are coordinated with superluminal ejections in the Seyfert galaxy, 3C120 (Marscher et al. 2002; Chatterjee et al. 2009; Lohfink et al. 2013). If one were to make an analogy between the GBHs and 3C120, the superluminal ejections in 3C 120 would have to be the equivalent of the discrete superluminal ejections in GBHs. However, superluminal discrete ejections in GBHs are characterized by very strong coronal emission in the last hours just before ejection that reach near historic maxima that can exceed 50% of the Eddington luminosity (Punsly and Rodriguez 2013). During the ejection, the X-ray luminosity becomes highly variable with an average value similar to that just before the ejection (Punsly and Rodriguez 2013). Thus, the claim of coronal X-ray power law luminosity dips in 3C 120 during superluminal ejections refers to a different phenomenon.

The corona X-ray power law emission during superluminal ejections in 3C 120 likely emerges from close to the black hole. However, there is no direct evidence that the emission from the innermost optically thick accretion flow is suppressed during superluminal ejections. The EUV emission from the high frequency tail of the optically thick thermal emission is not monitored. As noted above, in GBHs, the X-ray power law luminosity is not correlated with the optically thick thermal luminosity. Thus, there is no precedent that justifies the assumption that a dip in the X-ray power law equates to a dip in the optically thick thermal emission from the inner accretion disk in 3C 120. Thus, the physical state of the inner optically thick accretion disk during superluminal ejections is unknown. There is a claim of indirect evidence of inner disk movement outward during superluminal ejections based on Fe $K\alpha$ line width arguments derived from three X-ray observations (Lohfink et al. 2013). However, the interpretation of the X-ray data in the “high state” observed with XMM and the inner disk location claimed by Lohfink et al. (2013) disagrees with the seminal studies

of that data (Ballantyne et al. 2004; Ogle et al. 2005). The original studies of the XMM “high state” indicated that the Fe $K\alpha$ line was produced in cold plasma at $> 75R_g$ from the central black hole. This is very far from the innermost stable circular orbit where the cold plasma should reside if there were evidence of “a complete disk extending down to the innermost stable circular orbit (ISCO) during the XMM-Newton observation” as claimed by Lohfink et al. (2013).

The claim of evidence of an interaction of the jet with the corona during superluminal ejections in 3C 120 is not well understood, primarily because the corona is not a well understood region. There is strong evidence that the corona might be an out-flowing wind in Seyfert galaxies (Liu et al. 2014; Kharb et al. 2015). Does the corona envelope the disk like a stellar corona, or is it a separate optically thin radiatively inefficient disk inside the accretion disk, the so-called truncated disk scenario (e.g., Lohfink et al. (2013))? The physical interpretation of the depressed coronal emission is highly dependent on the model of the corona.

In summary, both GBHs and RLQs show a suppression of the optically thick thermal emission when jetted phenomenon occur. The Seyfert galaxy, 3C 120, shows something similar, but it is the coronal emission that appears suppressed which does not occur in GBHs. It would be a major advance if these three phenomena could be connected. There are many poorly understood details that would need to be studied and clarified further before we are at that point.

5. Conclusion and Future Prospects

This paper studies archival data on the distant quasar, 1442+101. Evidence of a real time connection between the jet power and the suppression of EUV emission is found. The result is based on only 5 epochs and simultaneity was established only within a 300 day interval. These findings motivate the need for a long term monitoring program of this source and other high redshift GPS. The radio observations would be improved with multi-frequency observations with VLA or ATCA. Knowing the flux density at more than one frequency (perhaps 8.4 GHz, 15 GHz and 22 GHz) would allow one to compute the luminosity of the optically thin emission and would be less prone to errors induced from slight changes in spectral slope that are problematic with a single frequency proxy. Coordinated sampling two times a year would be sufficient. Ideally, the source should be monitored with the same optical and radio instrument to minimize uncertainties in this difficult measurement. The VLA “gold sample” implemented here improves the situation, but there are still multiple optical telescopes involved.

We would like to thank Tracy Clarke for supplying the VLA data from September 30, 2011. We would also like to thank Patrick Ogle and Robert Antonucci for their valuable analysis of the 3C 120 X-ray data. BP notes that this research was supported by ICRANet.

REFERENCES

- Avara. McKinney, J. and Reynolds, C. <http://arxiv.org/abs/1508.05323>
- Ballantyne, D. R., Fabian, A. C., and Iwasawa, K. 2004 MNRAS 354 839
- Baldwin et al. 1974 ApJ 104 513
- Barthel, P. D., Tytler, D.R., Thompson, T.. 1990 Astron. & Astrophys. Supp. 82 339
- Baumann, G., Galsgaard, K. & Norlund, A., 2013 Solar Physics 284 467
- Blandford, R. and Znajek, R. 1977 MNRAS 179 433
- Blandford, R. D. and Payne, D., 1982 MNRAS 199 883
- Chatterjee, R., et al. 2009 ApJ 704 1689
- Corbin, M. 1991 ApJ 375 503
- Dallacasa, D., Fanti, C. Fanti, R., Schilizzi, R. and Spencer, R. 1995 A & A 295 27
- Davis, S., Laor, A. 2011, ApJ 728 98
- deVries, W., Becker, R., White, R. 2006, AJ 131 666
- Fender, R., Belloni, T., Gallo, E. 2004, MNRAS 355 1105
- Fuchs, Y. et al, 2003, A and A **409** L35
- Grier, C., et al. 2012, ApJ 755 60
- Haba et al. 2003, ApJ 599 949
- Igumenshchev, I. V. 2008 ApJ 677 317
- Kharb, P., Das, M., Paragi, Z., Subramanian, S., Chitta, L. P., 2015, ApJ 799 161
- Klein-Wolt et al., 2002, MNRAS 331 745
- Kovalev, Y. et al. 2004 A & A Supp 139 545

- Lind, K., Blandford, R. 1985 ApJ 295 358
- Liu, T., Wang, J-X, Yang, H., Zhu, F-F, Zhou, Y-Z, 2015 ApJL 783 106
- Lohfink, A. et al. 2013 ApJ 772 83
- Lovelace, R. V. E. 1976 *Nature* 262 649
- Lyons, R., Cohen, R., Junkkarinen, V., Burbidge, E. 1995 AJ 110 1541
- Lynden-Bell, D., Rees, M. 1971, *Mon. Not. R. Astr. Soc. Lett.* 152 461
- Malakit, K., Cassak, P., Shav, M., Drake, F. 2009, Geophysical Research Letter 36 L07107
- Mantovani, F.; Mack, K.-H.; Montenegro-Montes, F. M.; Rossetti, A.; Kraus, A. 2009 A & A 502 61
- Marscher, A., Jorstad, S., Gomez, J.-L., Aller, M. F., Terasranta, H., Lister, M., Stirling, A., 2002, *Nature* 417, 625
- Markov, S., Nowak, M., Wilms J. 2005, ApJ 635, 1203
- Marshall, H. 1997, ApJ 479, 222
- McKinney, J., Tchekhovskoy, A., Blandford, R. 2012 MNRAS 423 3083
- Mingaliev, M. G.; Sotnikova, Yu. V.; Torniainen, I.; Tornikoski, M.; Udovitskiy, R. Yu. 2012 A & A 544 25
- Mirabel, I.F. et al. 1998, A & A 330 L9
- Murphy, D., Browne, I.W.A., Perley, R.. 1993 MNRAS 264 298
- O’Dea, C. 1998 PASP, 110, 493
- Ogle, P. M., Davis, S. W., Antonucci, R. R. J., Colbert, J. W., Malkan, M. A., Page, M. J., Sasseen, T. P., Tornikoski, M., 2005 ApJ 618 139
- Pica, A. et al 1988 AJ 96 4
- Punsly, B. 2008, *Black Hole Gravitohydromagnetics*, second edition (Springer-Verlag, New York)
- Punsly, B. 2014 ApJL 797 33

- Punsly, B. 2015 *The Formation and Disruption of Black Hole Jets*, ASSL, 414 ISBN 978-3-319-10355-6. Springer International Publishing Switzerland, p. 149
- Punsly, B. 2015 ApJ 806 47
- Punsly, B., Rodriguez J. 2013, ApJ 764 173
- Punsly, B., Igumenshchev, I. V., Hirose, S. 2009 ApJ 704 1065
- Punsly, B. and Marziani 2015 MNRAS Lett 453 16.
- Pushkarev, A. and Kovalev, Y. 2012 A & A 544 34
- Russell, D. et al 2011 ApJL 739 19
- Shakura, N., Sunyaev, R. 1973, A & A 24 337
- Shimmins, A., Bolton, J. 1981, Aust. J. Phys. 34 471
- Smith, A., Nair, A., Leacock R., Clements S. 1993, AJ 105 437
- Stanghellini, C., O’Dea, C. P., Baum, S. A., Dallacasa, D., Fanti, R., Fanti, C 1997 A & A 325 943
- Stanghellini C., O’Dea C.P., Dallacasa D., Baum S.A., Fanti R., Fanti C. 1998 A & A Supp. 131 303
- Stanghellini, C., Dallacasa, D., O’Dea, C. P., Baum, S. A., Fanti, R., Fanti, C. 2001 A & A 377 377
- Steppe, H.; Jeyakumar, S.; Saikia, D. J.; Salter, C. J. 1995, A & A Supp. 113 409
- Tchekhovskoy, A., Narayan, R. and McKinney, J. 2011 MNRAS Lett. 418 79
- Tchekhovskoy, A., McKinney, J. 2012, MNRAS Letters 423 55
- Telfer, R., Zheng, W., Kriss, G., Davidsen, A. 2002 ApJ 565 773
- Threlfall, J. et al 2012, A & A 544 24
- Tingay, S. et al. 2003 PASJ 55 351
- van Breugel, W., Miley, G., Heckman, T. 1984 AJ 89 5
- Willott, C., Rawlings, S., Blundell, K., Lacy, M. 1999 MNRAS 309 1017

Yamada, M. 2007, *Physics of Plasmas* 14 058102

Zhu, Y. et al. 2012, *MNRAS* 424 2504